Arachidin-1 and Arachidin-3 Modulation of Rotavirus-infected MA104 Cells

Caleb M. Witcher
Stephen F Austin State University

Rebekah Napier-Jameson
Stephen F Austin State University

Hannah N. Lockwood
Stephen F Austin State University

Macie N. Mattila
Stephen F Austin State University

Stormey B. Wisdom
Stephen F Austin State University

Authors

Caleb M. Witcher, Rebekah Napier-Jameson, Hannah N. Lockwood, Macie N. Mattila, Stormey B. Wisdom, Luanna L. Saade Ferreira, Josephine Taylor, Beatrice Clack, Fabricio Medina-Bolivar, Judith M. Ball, and Rebecca D. Parr

Arachidin-1 and Arachidin-3 Modulation of Rotavirus-infected MA104 Cells

Caleb M Witcher[1, 2], Rebekah Napier-Jameson[1,3], Hannah N Lockwood[1,4], Macie N Mattila[1,5], Stormey B. Wisdom[1], Luanna L. Saade Ferreira[1], Josephine Taylor[1], Beatrice Clack[1], Fabricio Medina-Bolivar[6], Judith M Ball[7] and Rebecca D Parr[1*]

[1] Department of Biology, Stephen F Austin State University, Nacogdoches, TX 75962; [2] Ross University School of Veterinary Medicine, St. Kitts, West Indies; [3]Dedman College of Humanities and Sciences, Southern Methodist University, Dallas TX, 75235 [4] U.S. Dermatology Partners of Tyler, Tyler, TX, 75703; [5] Graduate School of Biomedical Sciences UT Health San Antonio, San Antonio, TX 78229-3900; [6] Department of Biological Sciences & Arkansas Biosciences Institute, Arkansas State University, Jonesboro, AR 72401; [7] Department of Biological and Environmental Sciences, Texas A&M University-Commerce, Commerce, TX 77843

Corresponding author: *e-mail: parrr1@sfasu.edu

ABSTRACT

Rotavirus (RV) causes severe life-threatening diarrhea in young children and immunocompromised individuals.   There are several licensed attenuated vaccines for young children, but there are no vaccines or antiviral therapeutics for immunocompromised patients of any age.   Previously, our laboratory demonstrated that arachidin 1 (A1) and arachidin 3 (A3) decreases the number of infectious simian RV particles and RV non-structural protein 4 (NSP4) in a human intestinal cell line which suggests effects on RV replication. This study examined the effects of the arachidins on the human RV (Wa)-infected African green monkey kidney cell line, MA104. The addition of either A1 or A3 did not decrease the viability of MA104 cells, however plaque forming assays measured significant decreases in the number of infectious RV particles with the addition of the arachidins. Correspondingly, western blot analyses revealed a change in the presence of VP6 and NSP4 (structural and nonstructural RV proteins, respectively). This implies that like the simian RV, Wa replication is also affected by both A1 and A3.   Additionally, tunable resistive pulse sensing technology (TRPS) measured changes in the population distribution of released nanoparticles between 60-140 nanometers. Additionally, TEM morphometric analyses showed ultrastructural changed in RV-infected cells treated with A1 or A3.   This included nucleus to cytoplasm ratios that were determined by TEM and whole cell fluorescent assays that disclosed significant nuclear size alterations with the addition of RV which implied modifications of the apoptosis and autophagy pathways. Moreover, the increased presence of autophagic vesicles seen with RV+A1 reinforced the model of a switch from the apoptosis to the autophagy pathway. In addition, immunoblot assays reveal the presence of cannabinoid 1 and 2 receptors on MA104 cells. These receptors bind A1 and A3 and are important in signaling in the endocannabinoid system. This implies a role for

1

A1 and A3 in modulating cannabinoid receptor cell signaling in RV-infected cells which indicates a mechanism of action of A1 and A3 with potential RV therapeutic activity.

INTRODUCTION

Rotaviruses (RV) are members of the Reoviridae family that causes infantile gastroenteritis in children less than 5 years of age (Ward, 1996), and severe diseases in pediatric and adult immunocompromised individuals (Anderson & Weber, 2004; Bakare et al., 2010; Park et al., 2015; Patel et al., 2010; Yin, Metselaar, Sprengers, Peppelenbosch, & Pan, 2015). There are two licensed RV attenuated vaccines, RotaTeq® (Merck) and Rotarix® (GlaxoSmithKline), in the United States that prevent severe diarrhea (Leshem et al., 2014; Yen et al., 2014), and an attenuated RV vaccine, Rotavac®, in India (Bhandari et al., 2014). However, the vaccines efficacies are dependent on the timing of vaccination, and are designed to protect against common RV strains (Jiang et al., 2010; Patton, 2012). Their efficacies are dependent on the genetic stability of the attenuated virus vaccines strains (Patton, 2012), but RV reassortments between RV strains are common and result in new infectious RV strains (Patton, 2012; Weinberg et al., 2013). This could produce RV strains that are not affected by the vaccine strains. Furthermore, the vaccines are contraindicated for immunosuppressed individuals, and there are no antiviral therapeutic agents currently available for RV infections. Besides the possibility of contracting RV-induced diarrhea directly from the infected individuals, there are documented cases of horizontal transmission of vaccine RV among immunocompromised household contacts from vaccinated children who shed the vaccine virus (Hsieh et al., 2014; Patel et al., 2010; Yen et al., 2015). Development of effective antiviral drugs that affect a wide-range of RV strains and reduces the burden of disease is an important strategy for the prevention of RV disease, especially in immunocompromised individuals. Likewise, the discovery of the antiviral mechanism(s) could lead to the development of compounds with a broad range of antiviral activity.

Our laboratory is investigating the effects of highly purified stilbenoids extracted from peanut (*Arachis hypogea*) hairy root cultures on RV infections (Ball et al., 2015). Stilbenoids are secondary metabolites derived from plants that have antioxidant, anticancer, antifungal and anti-inflammatory properties, and have shown many potential human health benefits (Aggarwal et al., 2004; Athar et al., 2007; Roupe et al., 2006; Yang et al., 2017). They are products of the phenylpropanoid/acetate pathway and act as phytoalexins produced by plants such as grapes, berries, and peanuts in response to pathogens (Huang et al., 2010; Moss et al., 2013). Two prenylated stilbenoids, arachidin 1 (A1) and arachidin 3 (A3), significantly inhibit the production of infectious simian RV (SA114f) and show a reduction in the viral nonstructural protein, NSP4, which is critical for viral replication (Ball, et al., 2015). Other studies have demonstrated that the activation of cellular signaling pathways is dependent on the RV strains and cell lines used in their experiments (Di Fiore et al., 2015; Halasz et al., 2010; Holloway et al., 2009; Holloway and Coulson, 2006; Otto et al., 2015; Saxena et al., 2016; Uzri and Greenberg, 2013).

This study shows significant changes in the number of infectious human RV (Wa) particles produced with the addition of either A1 or A3 on the African green monkey kidney cell line, MA104. Correspondingly, western blot assays show changes in the presence of both structural and nonstructural RV proteins, VP6 and NSP4, respectively, suggesting an effect on progeny RV particles and replication. Additionally, tunable resistive pulse sensing technology (TRPS) using the qNano system by Izon revealed different patterns in the size

distribution of nanoparticles released from the arachidin treated, RV-infected MA104 cells. Transmission electron microscopy (TEM) was used to observe morphometric changes between the RV-infected arachidin-treated cells, and the changes observed in the ratios of the nucleus to cytoplasm were substantiated with fluorescent-labeled whole cell assays.

It is known that A1 and A3 bind to cannabinoid receptors which are important in the control of the endocannabinoid system. In this study, we revealed the presence of cannabinoid receptors 1 and 2 on MA104 cells. This implies a role for A1 and A3 in modulating cannabinoid receptor cell signaling in RV-infected cells suggesting a mechanism of action of A1 and A3 with potential RV therapeutic activity

MATERIALS AND METHODS

Cell lines and virus. MA104 cells were obtained from ATCC (Rockville, MD) and maintained in Eagle Modified Essential Medium (MEM; Gibco, Grand Island, NY) supplemented with 5% fetal bovine serum (FBS), glutamine (2 mM), penicillin-streptomycin (100 µg/mL) and non-essential amino acids (Sigma, St. Louis, MO as a 100X solution. The amino acids were used at a 1X concentration of 100 µM each.) (Mitchell and Ball, 2004). The cell line was confirmed to be free of mycoplasma contamination using the MycoFind mycoplasma PCR kit version 2.0 (Clongen Laboratories, LLC). RV Wa (G[1] P[8] genotype) was amplified (Matthijnssens et al., 2008). Viral titers on virus stocks were determined in MA104 cells, followed by storage at -80°C. Arachidin 1 and 3 efficacies against RV were tested using MA104 cells.

Bioproduction of stilbenoids in hairy root cultures of peanut. Stilbenoids were produced as previously reported using the established hairy root line 3 from peanut cv. Hull (Condori et al., 2010) that was stimulated with the elicitor methyl-β-cyclodextrin

(CD) (Cavasol® W7M) (Yang et al., 2015). A 72-hour treatment of 9 g/L CD was selected based on the highest production of A1. At day nine of the hairy root culture, the spent medium from each flask was removed and replaced with elicitation medium (fresh MSV medium with 9 g/L methyl-β-CD and incubated in the dark at 28°C for an additional 72 h to induce synthesis and secretion of stilbenoids into the culture medium as recently described (Yang et al., 2015). After the elicitation period, the culture medium was removed from each flask and combined. This pooled medium was mixed with an equal volume of ethyl acetate in a separatory funnel to extract the stilbenoids as described previously (Condori et al., 2010). The ethyl acetate phase was recovered and was dried in a rotavapor (Buchi), and A1 and A3 were purified from the extract by HPCCC as follows. The dried ethyl acetate extract was suspended in HPCCC solvent system (hexane: ethyl acetate: methanol: water [4:5:3:3]) and injected into a Spectrum™ (Dynamic Extractions) HPCCC system. HPCCC fractions containing A1 and A3 with over 95% purity based on HPLC analysis (UV 340 nm) were combined, dried under a nitrogen stream and used for viral assays (Ball et al., 2015). As previously demonstrated, A1 and A3 were the major stilbenoids present in the culture medium, and the dry mass of each stilbenoid was reconstituted in 0.02% DMSO in MEM medium (Ball et al., 2015).

Viability Assay. Viability assays were performed as previously described using the Trypan blue cell exclusion assays (Ball et al., 2015; Freshney, 1994). MA104 cells were grown to 80% confluence in 6-well tissue culture plates (Corning Life Sciences) and starved for fetal bovine sera 12 hours prior to the addition of RV alone, DMSO alone, RV + DMSO, RV + 20 µM A1, RV + 20 µM A3, 20 µM A3, 20 µM A1 and NV (no virus). At 18 hours post infection (hpi) a suspension of 10^6 cells/ml was diluted 1:1 with a 0.4% Trypan blue solution and loaded onto a hemocytometer. The number of stained cells and

total number of cells were counted, and the calculated percentage of unstained cells was reported as the percentage of viable cells. Each treatment was performed in triplicate, and data was expressed as the mean +/-standard deviation (SD). Comparisons were statistically evaluated by a one-way analysis of variance (ANOVA) and Student's t two tailed tests using Excel (significance level, $p \leq 0.05$).

RV Infections. To test the biological activity of the stilbenoids on RV infections, MA104 cells were grown to 80% confluence in 6 well tissue culture plates (Corning Life Sciences), starved for fetal bovine sera twelve hours prior to infection and then infected with RV (Wa) as previously described (Arnold et al., 2009; Ball et al., 2015; Yakshe et al., 2015). Rotavirus (Wa) stocks were sonicated for five minutes using a cup horn attachment with a Q500 Sonicator (QSonica Sonicators, Newtown, CT), and incubated in serum-free MEM with 1 µg/mL trypsin (Worthington Biochemical, Lakewood, NJ) for 30 min at 37°C. The activated viral inoculum was incubated with cells for 1 h at 37°C in 5% CO_2 at multiplicity of infection (MOI) of 2. The inoculum was replaced with serum-free MEM supplemented with 1 µg/mL trypsin and incubated for 18 hpi. The supernatants were collected, clarified at 300 x *g* for 5 min, and stored at -80°C for plaque assays and TRPS analysis (see below). The cells were washed in cold 1X Dulbecco's PBS (Caisson Laboratories, Smithfield, UT), and released from the plates using a 0.25% Trypsin-EDTA Solution (Caisson Laboratories, Smithfield, UT). After the addition of MEM with 5% FBS, the cells were suspended in cold 1X PBS and dilutions were prepared for live/dead cell counts (see above in Viability Assays). For TEM analysis, approximately 2 x 10^6 cells were washed in cold 1X PBS, fixed with 5% glutaraldehyde and used for TEM analysis as described below.

Infectious RV quantification. PFU assays were performed in triplicate as previously described (Arnold et al., 2009; Ball et al., 2015; Yakshe et al.,

2015). Briefly, ten-fold dilutions of RV alone and RV with 0.002% DMSO and 20 µM A1 or A3 were added to the serum starved MA104 cells for one hour as described above. The virus inoculum was replaced with 3 mL of a medium overlay (1:1 mixture of 1.2% agarose [Apex Low Melting Point Agarose, Genesee Scientific Inc] and complete MEM containing 0.5 µg/mL trypsin and incubated at 37°C in 5% CO_2 for 3 to 4 days or until plaques became visible. A neutral red overlay (1:1 mixture of 1.2% agarose with an equal volume of serum-free MEM containing 50 µg/mL neutral red) was prepared and 2 mL per well of stain overlay was added on top of the first agarose/medium overlay. The six-well plates were incubated at 37°C until plaques were visible (approximately 12 to 72 h). The individual plaques were counted, and the titers were calculated as follows: Number of plaques x 1/dilution factor x 1/ (mL of inoculum) = PFU/mL. Plaque forming assays were performed in triplicate with data are expressed as mean +/-SD. Comparisons were statistically evaluated by analysis of variance (ANOVA) and Student's t two tailed tests using Microsoft Excel 2011 software (significance level, $p \leq 0.05$).

Quantification and Size Distribution of RV Particles. To determine the concentration and size of nanoparticles released from the treated samples (RV, RV+A1 and RV+A3), TRPS analysis using the qNano system (Izon Science, Cambridge, MA) was employed. TRPS is based on a coulter counter that is composed of two fluid reservoirs filled with an electrolyte or other conductive media and separated by a membrane containing a pore (Kozak et al., 2011; Weatherall et al., 2016). When an electrical field is applied across the pore, the resistance to the resulting ionic current is indirectly proportional to the cross-sectional area of the pore. When a non-conducting particle passes through the pore, the increase in resistance is proportional to the particle volume relative to pore size. This change in resistance is detected as a pulse in an ionic current. The pulse

frequency is proportional to particle flow rate and particle concentration (DeBlois and Bean, 1970). This system provides a quick and accurate way to measure individual sizes of nanoparticles and their volume in a solution (Farkas et al., 2013; Vogel et al., 2011). All qNano experiments were performed using the manufacturer's established protocols (Bo et al., 2014; Jones, 2015; Vogel et al., 2011). Prior to counting and measuring the particles, samples were purified using a qEV size exclusion column from Izon that contains a resin with an approximately 75 nm pore size. The purified particles samples were suspended in PBS with 0.025% Tween 20 to reduce particle aggregation and ease the wetting of the nanopore. Dilutions of 1:1000 of the samples were placed on the qNano size-tunable nanopore (NP100, Izon), and each sample was measured as a transient change in the ionic current flow. This was denoted as a blockade event with its amplitude representing the blockade magnitude. Because the blockade magnitude is proportional to the particle size, accurate particle sizing was achieved after calibration with 100 nm particles (CPC100B, Izon) using identical settings. The size distribution and concentration analyses were performed using IZON Science proprietary software v3.2.2.268.

Morphometric analysis of RV-infected MA104 cells. TEM analysis was performed on RV-infected MA104 cells to visualize the effects of the A1 and A3 on progeny virus and cellular morphology. Samples were prepared as described (Wright, 2000). RV-infected MA104 cells with and without 20 µM A1 or A3 were incubated for 18 hpi, washed with PBS and then trypsinized. Cells were pelleted and fixed with 5% glutaraldehyde overnight at 4°C. The cells were post-fixed with 2% osmium tetroxide, dehydrated with a graded ethanol series (15 - 30 minutes incubation of the following: 30%, 50%, 70%, 80%, 90%, and 100% ethanol), infiltrated and embedded in Spurr's resin. Thin sections were stained with uranyl acetate and lead citrate and were

examined with a Hitachi H-7000 electron microscope operating at 75 KeV. Negatives were digitized at 1200 dpi and analyzed using Macnification Version 2 (Orbicule, Inc., www.orbicule.com). RV particles were observed in RV-infected cells, and the average diameters of enveloped and non-enveloped particles were measured (n=23 particles for each group; the data was expressed and graphed as the mean +/- SD. Also, the mean the cell nucleus to cytoplasm ratios were determined using twelve micrographs of six treatment groups (No virus, RV, RV+A1, RV+A3, A1, A3). All data were presented as the mean ± standard deviation. Statistical analyses were performed using one-way analysis of variance followed by Bonferroni's post hoc test using Excel. P<0.05 was considered to indicate a statistically significant difference.

W1Xhole cell fluorescent labelling of nucleus and plasma membranes. The nucleus and plasma membranes of MA104 cells were fluorescently labelled to determine the ratios of the nucleus to cytoplasm of whole cells to compare to the nucleus to cytoplasm ratios obtained with TEM. Briefly, MA104 cells were grown to 80% confluence in 8-well slides (Lab-Tek Chamber Slide System, Nunc, Inc. Naperville, IL) and RV-infected and treated with the arachidins as described above (RV alone, RV with 20 µM A3 or A3, 20 µM A1 alone, or 20 µM A3 alone, and cells without treatments (NV-no virus). At 18 hpi, the cells were washed with 1X PBS one time at 25°C, and then fixed with 1% Glutaraldehyde (Electron Microscopy Science, Hatfield, PA) for one hour at 25°C in a fume hood (Harlow and Lane, 1988). Following fixation, the cells were washed twice with 1X PBS at 25°C. The Image-IT™ LIVE Plasma Membrane and Nuclear Labeling Kit (I34406) (Molecular Probes, Invitrogen detection Technologies, Eugene, OR) was used to label the cells. Briefly, one solution for the single step staining for both stains was prepared by adding

5.0 µg/mL Alexa Flour 594-labeled wheat germ agglutinin and 1 µM Hoechst 33342 stain into 1X PBS. One-hundred µLs of the labelling solution was added to each well in 8-well chambered slides, and incubated for ten minutes at 25ºC, removed and the cells were washed twice with 1X PBS, and mounted in 1X PBS. The microscopic analysis was carried out using the Olympus BX50 with DP Manager System compound light microscope with epifluorescence illumination for Alexa Fluor 594 labeled wheat germ (Excitation 480-550nm, dichroic mirror DM 570nm, barrier filter 590nm) and Hoechst 33342 (Excitation 330-385nm, dichroic mirror DM 400nm, barrier filter BA420nm) with the DP71 camera (Olympus Corporation, Shinjuku, Tokyo, Japan) equipped with x 40 and X100 objectives. The images were digitized using the DP Controller software (Olympus Corporation), and the pixels of the nucleus and whole cell were measured using Macnification Version 2 (Orbicule, Inc., www.orbicule.com). Excel was used to determine the nucleus to cytoplasm ratio of the cells of 45 to 56 cells per treatment. Data are presented as the mean ± standard deviation. Statistical analyses were performed using one-way analysis of variance followed by Bonferroni's post hoc test using Microsoft Office Excel 2016 software. $P<0.05$ was considered to indicate a statistically significant difference.

Western blot and Immunoblot assays. For western blot analyses of RV proteins, 20 µg (to detect VP6) and 1 µg (to detect NSP4) of cell lysates were prepared and quantified as described above, separated by 12% SDS-PAGE, and electroblotted onto nitrocellulose membranes. The membranes were probed with a 1:1000 dilution of polyclonal rabbit serum anti-NSP4 (150-175) or polyclonal rabbit anti-VP6 specific antibodies (a gift from Dr. Judith M Ball), and reactive bands were visualized by the addition of 1: 5000 dilution (0.2ng/µl) HRP-conjugated donkey anti-rabbit IgG (GE Health Sciences) with the addition of the Prometheus

Protein Biology Products ProSignal Femto ECL Reagent (Genesee Scientific). The digital images were captured using the Amersham Imager 600 (GE Healthcare UK Limited Amersham Place Little Chalfont Buckinghamshire HP7 9NA United Kingdom). The expression of GAPDH was used as a loading control on all western blots. Rabbit anti-GAPDH (PA1-988, Thermo Fisher Scientific, Waltham, MA) was incubated at a 1: 5000 dilution (0.2ng/µl) and visualized for the viral proteins, VP6 and NSP4, as described above for GAPDH.

Cell lysates were prepared from treated and untreated MA104 cells, and total protein was quantified using a micro-BCA protein assay as previously described (Ball et al., 2015). For immunoblot assays, two-fold dilutions of RV-infected and noninfected MA104 cell lysates (10, 5, 2.5, 1.25 µg) were added to nitrocellulose membranes using a slot blot apparatus (Bio-Rad). Membranes were blocked with 10% nonfat dry milk and probed with a 1 µg/mL of rabbit anti-CNR1/2 antibodies from Assay Biotechnology (Sunnyvale, CA), and incubated with 8 ng/mL of goat anti-rabbit IgG (H&L) Alexa Fluor 546 (Invitrogen, Carlsbad, CA). Goat anti-rabbit Alexa Fluor®546-labelled antibodies (Life Technologies) were added and reactive bands were visualized using the 556 nm excitation laser and 573 nm emission filter on the Typhoon 9500 Plus laser scanner (GE Life Sciences, Marlborough, MA).

RESULTS

Viability of RV-infected MA104 cells in the presence of DMSO, A1, and A3.
At 18 hpi, RV-infected cells showed an average viability of 89.46% (STD dev ± 5.6) and RV+0.002% DMSO showed 91.5% (STD dev ± 5.2) cell viability. Cells treated with RV+20 µM A1 displayed a viability of 90% (std dev ± 0.6) and 20 µM A1 alone had a 91.3% (std dev ± 2.6) viability. Cells treated with RV + 20 µM A3 displayed a

viability of 92.5% (std dev ± 2.6) and 20 µM A3 alone had a 95.8% (std dev ± 2.6) viability. Untreated cells (no virus - NV) demonstrated 93% (std dev ± 2.6, and NV+0.002% DMSO showed a viability of 97.5% (std dev ±0.58). There were no statistical differences between all treatments except RV+A1 was statistically different from A3 (P = 1.11E-4) and NV+0.002% DMSO (P = 1.31E-5) (Figure 1).
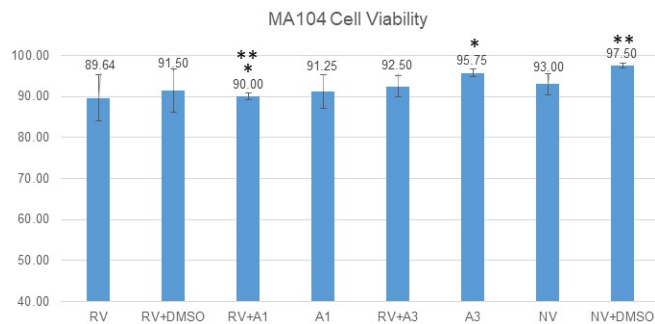

Figure 1. **MA104 cell viability assay.** Trypan blue exclusion assays were performed in triplicate (RV, RV+0.002% DMSO, RV 20µM A1, 20µM A1, RV+20 µM A3, 20 µM A3, NV-no virus and NV+0.002% DMSO) at 18 hpi. The mean percent live/dead cells were calculated. Data were expressed as the mean ± SD, and comparisons were statistically evaluated with a one-way ANOVA and two-tailed Students' t-tests followed by Bonferroni's correction using Microsoft 2016 Excel software (significance level, P <0.05). *Statistically different (RV+A1/A3) with P = 1.11E-4. **Statistically different (RV+A1/NV+0.002% DMSO) with P = 1.31E-5.

The effects of A1 and A3 on the production of infectious RV particles.
Supernatants were collected at 18 hpi from the RV-infected and RV-infected with 20 µM A1 or A3 and used for plaque forming assays to quantify infectious RV particles. Plaques were counted and the average of three experiments was calculated and graphed as PFU/mL (Figure 2). The PFU assays demonstrated a statistical difference in the production and release of infectious viral particles with the addition of A1 and A3. At 18 hpi, RV only had a titer of 3.9E11, RV+A3 had a titer of 6.67E9, and RV+A1 had a titer

of 7.11E9 (Figure 2). This demonstrates a 59-fold and 55-fold reduction in PFU/ml in RV+A3 and RV+A1, respectively resulting in P = 1.356E-07 for both arachidins when compared to RV. Both RV+A3 and RV+A1 showed no statistical difference from each other (P = 0.3731).
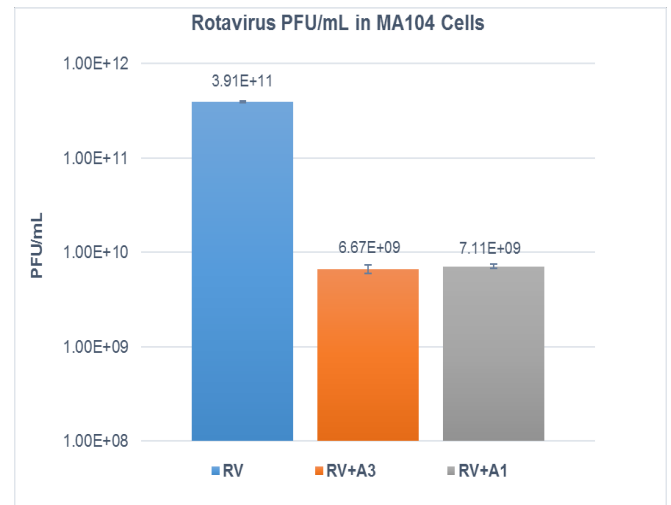

Figure 2. **Plaque forming assays using supernatants from RV-infected and arachidin treated MA104 cells.** MA104 cells were infected with Wa RV (Wa) at an MOI of 2 and treated with 20 µM A1 or A3. At 18hpi, the cell supernatants were collected, centrifuged, and serial diluted for plaque forming assays to determine the number of infectious viral particles/mL as plaque forming units (PFU/ml). Comparison of RV to RV+A1 and RV to RV+A3 both P = 1.356E-7.

TEM viral particle size analyses of rv-infected ma104 cells.
The presence of enveloped and nonenveloped RV particles was demonstrated in micrographs with a scale bar of 0.25 microns, and the less mature enveloped RV particle was shown entering the ER from a viroplasm (Figure 3A). The average diameters of enveloped and non-enveloped RV particles were measured (n=20 particles for each group) (Figure 3B). The less mature enveloped RV particles had a mean diameter of 112.736 ±3.20 and the more mature nonenveloped RV particles had a

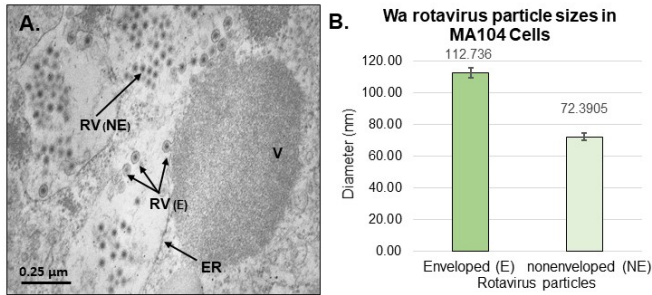mean diameter of 72.391 ± 2.172 nanometers which were statistically significant P = 1.2366E-34 (Figure 3B).

Figure 3. **Transmission electron micrograph (TEM) of Wa rotavirus infected MA104 cells at 18hpi**. Final Magnification = 57,000x. A) Endoplasmic reticulum (ER), Viroplasm (V), Enveloped virus particles (E), and non-enveloped virus particle (NE). B) Measurements of RV particles in TEM micrographs of MA104 cells infected with Wa rotavirus at 18 hpi (n = 20 per group). Enveloped RV particles averaged 112.736 ± 3.20 nanometers in diameter, and nonenveloped RV particles averaged 72.391 ± 2.172 nanometers in diameter (statistically significant P = 1.236E-34).

TEM morphometric analyses of MA104 cells. Morphometric analyses using twelve TEM micrographs of each treatment groups. The uninfected (NV-no virus), 20 µM A1 and 20 µM A3 only treated MA104 cells were compared to RV infected cells as well as infected cells treated with A1 or A3 at 18 hpi. The three controls groups, no virus (NV), 20 µM A1, and 20 µM A3 (Figure 4A, 4B and 4C, respectively) showed similar morphology. Conversely, the RV-infected cells demonstrated an increase in the size of the nucleus, many cytoplasmic vesicles and cytoplasmic blebbing (Figure 4D) which are characteristics of apoptosis (Elmore, 2007). However, RV-infected cells treated with A1 and A3 (Figures 4E and 4F, respectively) appeared to have a more normal sized nucleus, and RV-infected cells treated with A1 had many autophagosomes and large sized mitochondria-like organelles (M), while the A3 treated cells exhibited many small mitochondria-like organelles and many vesicles in the cytoplasm (Figures 4E and F).

TEM analyses of MA104 cell nucleus to cytoplasm ratios. The ratio of nucleus to cytoplasm was calculated using twelve representative cells from each treatment. At 18 hpi, the mean ratios of the control cells treated with A1 (0.44±0.218) and A3 (0.39±0.177) were like the cells with no treatment, NV (0.48±0.173) (Figure 5), while the RV-infected cells demonstrated an increased nucleus to cytoplasm ratio with a mean ratio of 1.31±0.347. RV-infected cells treated with A3 and A1 had mean ratios, 0.49±0.184 and 0.54±0.156, respectively, which were comparable to the ratios of the control cells. However, both arachidin, treated RV-infected cells displayed different ultrastructure characteristics than the control cells. RV-infected cells treated with A1 had many autophagosomes and large sized mitochondria, while the A3 treated cells exhibited many small mitochondria and many vesicles in the cytoplasm (Figure. 5).

Fluorescent labelling of nucleus and plasma membrane. MA104 cells treated with and without arachidins with and without RV were collected at 18 hpi, fixed, and incubated with Alexa Fluor 594 wheat germ agglutinin (WGA) and blue-fluorescent Hoechst 33342 dye for selective staining of the plasma membrane and nucleus, respectively. After the cells were observed using the Olympus BX50 with DP Manager System compound light microscope with epifluorescence, the pictures were digitized and the pixels of the nucleus and whole cell were measured using Macnification Version 2 (Orbicule, Inc., www.orbicule.com). Nucleus to cytoplasm ratios were calculated and statistical analyzed.
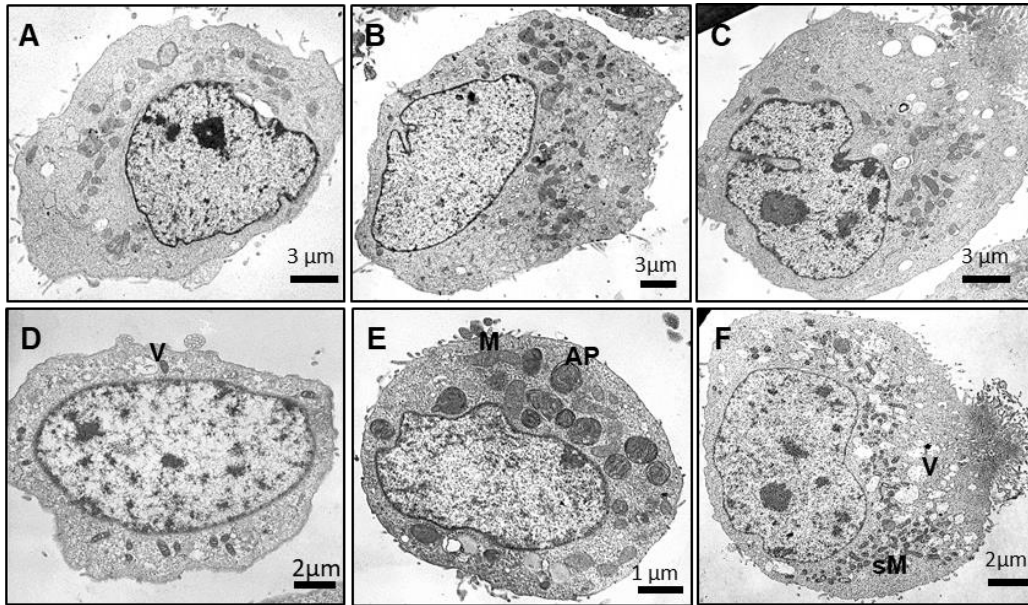
Figure 4. **Transmission electron micrograph (TEM) of Wa rotavirus (RV) infected MA104 cells at 18 hpi.** A) NV, no virus; B) A1 only; C) A3 only; D) RV only; E) RV+A1; F) RV+A3. Scale bars equal 1-3 microns. RV-infected cells (D) and RV+A3 (F) display many cytoplasmic vesicles (V) while RV+A1 has many autophagic vesicles (AP) and large mitochondria-like organelles (M). RV+A3 has many vesicles (V) and small mitochondria-like organelles (sM).
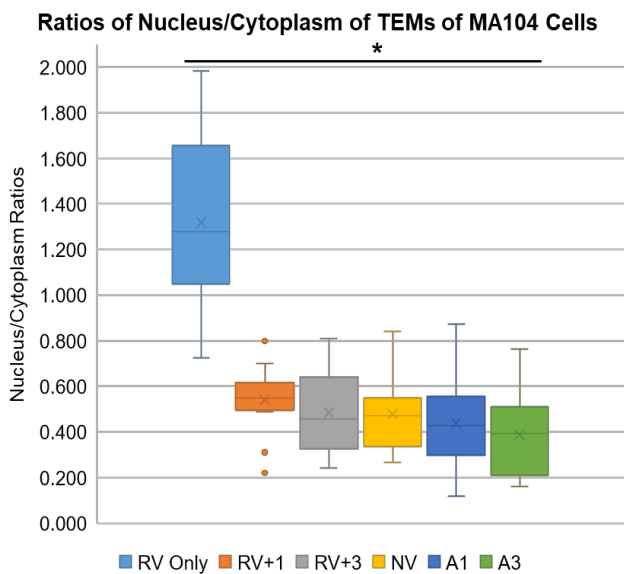

Figure 5. **TEM nucleus to cytoplasm ratios of MA104.** Cells were collected and processed for TEM analysis, and the areas of the nucleus and cytoplasm of ten micrographs for each treatment groups were measured with Macnification (Orbicule, Inc.). Nucleus to cytoplasm ratios were calculated and statistical analyses were performed. The data were analyzed by one-way analysis of variance (ANOVA) and two-tailed Student's t tests (significance level, $P < 0.05$) with Bonferroni's *post hoc* test to correct for multiple comparisons. The data was graphed using a whisker and box plots. The box represents all the data points within the lower (Q1) and upper (Q3) quartiles with vertical lines with an x that represents the median. The whiskers go from each quartile to the minimum and maximum data points. Data points falling outside the overall pattern of distribution were plotted as dots that represent outliers. * RV was statistically different from RV+A1 (P=1.738E-05); RV+A3 (P=7.203E-06); NV (P=6.787E-06); A1 (P=3.479E-06); and A3 (P=1.976E-06).

9

Quantification of RV particles and size distribution by TRPS analysis. TRPS analysis was performed on the RV infected cell supernatants (with and without treatments with A1 or A3) to display the concentration of virus particles/mL, diameter of RV particles and size distribution of particles. TRPS allow for high-throughput single particle measurements as virus particles are driven through pores, one at a time, causing a blockade event that can be measured for individual size; the number of blockades is used to determine the concentration (Vogel et al., 2011).
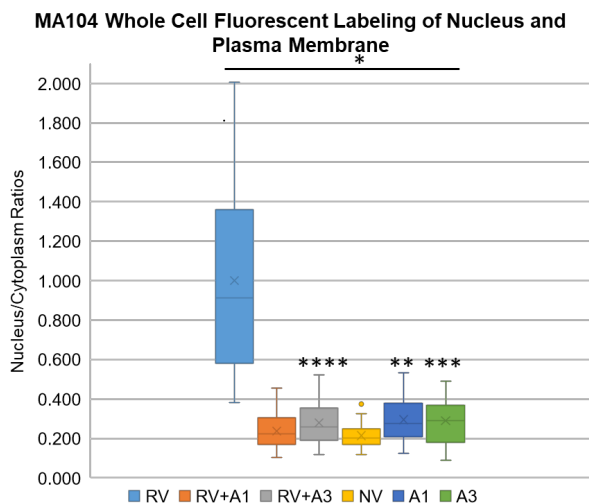
MA104 Whole Cell Fluorescent Labeling of Nucleus and Plasma Membrane

Figure 6. **Nucleus to cytoplasm ratios of whole MA104.** Cells were collected and fixed and stained with 5.0 µg/mL Alexa Flour 594-labeled wheat germ agglutinin to observe membranes and 1 µM Hoechst 33342 to visualize the nucleus. The microscopic analyses of 45-56 cells from each treatment groups were carried out using the Olympus BX50 microscope. The images were digitalized and the pixels of the nucleus (N) and whole cell were measured using Magnification Version 2 (Orbicule, Inc., www.orbicule.com). The N/Cytoplasm ratios were analyzed by one-way analysis of variance (ANOVA) and two-tailed Student's t tests (significance level, $P < 0.05$) with Bonferroni's *post hoc* test and graphed using a whisker and box plots. The box represents all the data points within the lower (Q1) and upper (Q3) quartiles with vertical lines with an x that represents the median. The whiskers go from each quartile to the minimum and maximum data points. Data points falling outside the overall pattern of distribution were plotted as dots that represent outliers. *RV was statistically different from RV+A1 (P=4E-22); RV+A3 (P=3.4E-20); NV (P=2.5E-21); A1 (P=3E-18); and A3 (P=1.4E-17). **NV was statistically different from A1 (P=1.4E-5); and ***NV was statistically different from A3 (P=5.5E-5). ****NV was statistically different from RV+A3 (P=0.0003).

The RV only samples showed a concentration of 1.71 x 10^{13} particles/mL at 18 hpi, and the particles had a dispersed range in diameter from approximately 60-120 nm (Figure 7A). At the same time, RV-infected cells treated with A3 showed a concentration of 4.25 x 10^{12} particles/mL with the particle size diameters between 90-140 nm (Figure 7B). Additionally, RV-infected cells treated with A1 displayed a concentration of 1.42 x 10^{12} particles/mL with a population of particles between 70-150 nm (Figure 7C). This reveals a shift in the size distributions of the populations of RV particles from a smaller size that is more consistent with mature infectious RV particles to larger, more immature RV particles with the addition of the arachidins.

Western blot assays to detect rotavirus proteins. Western blots were performed to visualize the presence of RV nonstructural protein 4, NSP4 assays as previously described (Parr and Ball, 2003; Parr et al., 2006; Zhou, 2004) and the RV structural protein, VP6, in RV-infected cell lysates with/without treatment with arachidin 1(A1) or arachidin 3 (A3). Rabbit polyclonal antiserum to the SA11 NSP4 synthetic peptide aa150-175 (αNSP4$_{150-175}$) and polyclonal antiserum to VP6 was kindly provided by Dr. Judith Ball (Texas A&M Commerce, Commerce, TX) and rabbit anti-GAPDH antibodies were obtained from Thermo Fisher Scientific (Waltham, MA). One microgram of the cell lysates was used for NSP4, and 20 µg of cell lysates were used to visualize VP6. Results showed a band at ~36 kDa for GAPDH and ~42 kDa for VP6 (Figure 8A) and displayed NSP4-specific bands ~28 and 56 kDa, and a GAPDH-specific band ~36 kDa (Figure 8B).
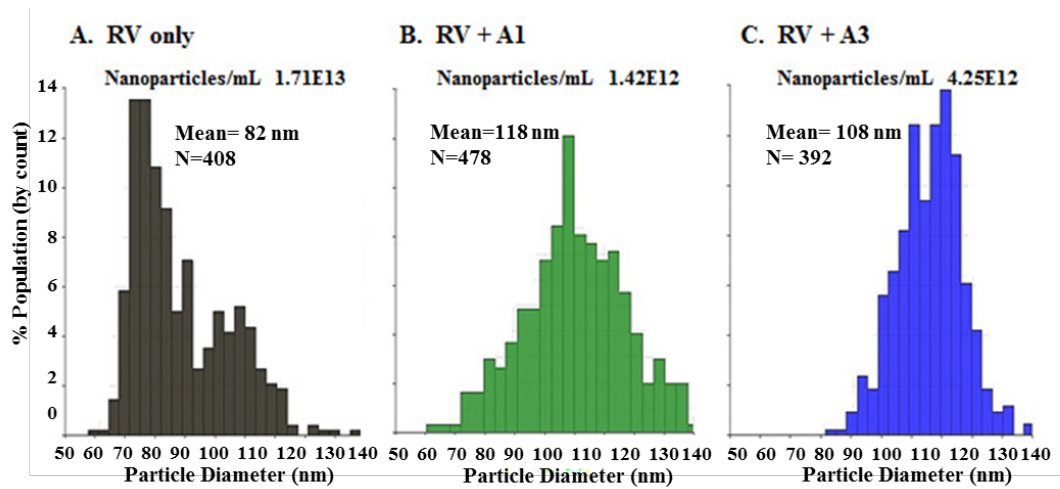
Figure 7. **TRPS analysis of arachidin treat MA104 cells.** The size variations, virus concentrations and population distribution of extracellular RV particles were measured from supernatants of RV-infected cells treated with/without A1 and A3 at 18 hpi. A) RV-infected supernatants, B) Supernatants from RV-infected cells treated with 20 µM A1, and C) Supernatants from RV-infected cells treated with 20 µM A3
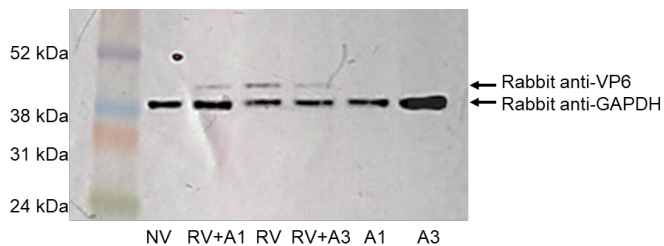

Figure 8A. **The detection of the rotavirus structural protein VP6 in MA104 cells.** Cell lysates (20 µg) were separated on a 12% SDS/PAGE gel, electroblotted onto a nitrocellulose membrane, and probed sequentially with a 1:1000 dilution of rabbit anti-VP6 antiserum and a 1:5000 dilution (0.2ng/µl) of donkey anti-GAPDH antibody. Amersham Rabbit IgG, HRP-linked whole donkey antibodies were added at a 1:5000 dilution (0.2ng/µl), and the chemiluminescent detection was performed using the Prometheus Protein Biology Products ProSignal Femto ECL Reagent (Genesee Scientific) and Amersham imager 600. Results show a band at ~36 kDa for GAPDH and ~42 kDa for VP6.
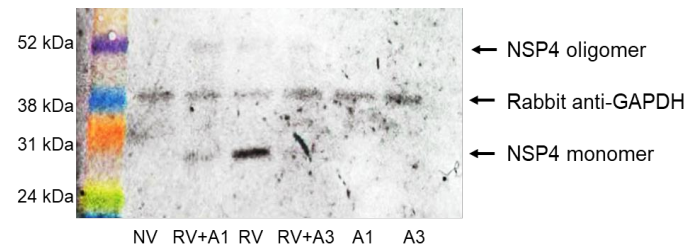
Figure 8B. **The detection of the rotavirus nonstructural protein NSP4 in MA104 cells.** Cell lysates (1 µg) were separated on a 12% SDS/PAGE gel, electroblotted onto a nitrocellulose membrane. The membrane was probed sequentially with a 1:1000 dilution of rabbit anti-NSP4 antisera and a 1:5000 dilution (0.2ng/µl) of rabbit anti-GAPDH antibody. Rabbit IgG HRP-linked whole donkey antibodies were added at a 1:5000 dilution (0.2ng/µl), and the chemiluminescent detection was performed using the Prometheus Protein Biology Products ProSignal Femto ECL Reagent (Genesee Scientific) and Amersham imager 600. Results showed a band at ~36 kDa for GAPDH and ~28 and 56 kDa for NSP4.

11

The presence of autophagy vesicles in rv infected ma104 cells treated with A1 or A3. MA104 cells from each treatment (n = 12 each) were scored positive or negative for the presence of autophagic vesicles as demonstrated in Figure 4E. Control cells (no virus – NV) showed autophagosomes in 23.1% of the observed cells, while 8.3% of the A3 alone treated cells and 66.7% of the A1 alone treated cells were positive for autophagic vesicles (Figure 9).
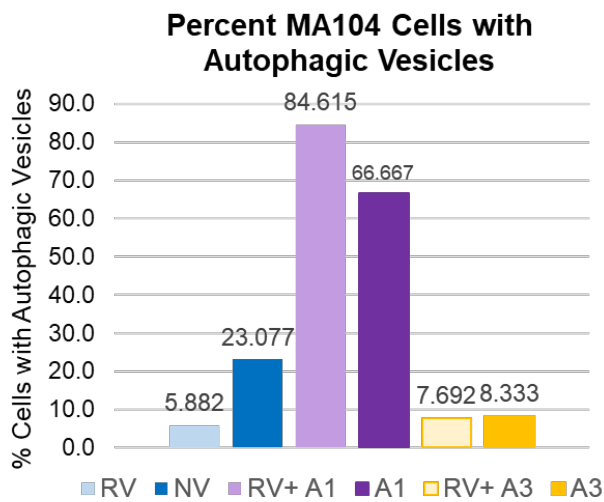

Figure 9. **Percent MA104 cells with autophagic vesicles at 18 hpi**. TEMs of RV-infected, RV-infected arachidin treated, A1 only, A3 and NV (no virus) cells were scored positive or negative for the presence of autophagic vesicles and the means for each treatment (n = 12) were compared in a graphed format..

Comparatively, 5.9% of the RV-infected cells, 84.6% of RV-infected cells treated with A1, and 7.7% of RV-infected cells treated with A3 were positive for autophagy vesicles (Figure 9).

Immunoblot assays to detect cannabinoid receptors. Immunoblot assays were performed to confirm the presence of both A) cannabinoid receptor 1 (CBR1) and B) cannabinoid receptor 2 (CBR2) on MA104 cells (Figure 10). Both uninfected cell lysates (Figure 10A lane 1 and 10B lane 1) and RV-infected cell lysates (Figure 10A lane 2 and 10B lane 2) were positive for both receptors, and there appears to be a stronger signal with both CBR1 and CBR2 antibodies from the RV-infected cell lysates (Figure 8A lane 2 and 8B lane 2).
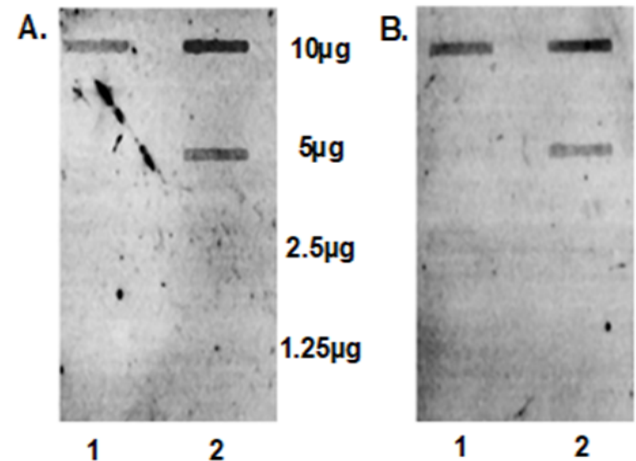

Figure 10. **Cannabinoid Receptors 1 and 2 on MA104 cells.** Two-fold dilutions of MA104 cell lysates (10 µg, 5 µg, 2.5 µg, 1.25 µg) were added to nitrocellulose membranes [1-uninfected and 2-RV (Wa)-infected], probed with a 1:1000 dilution (1 ng/µl) of rabbit anti-CBR1 (A) or anti-CBR-2 (B) antibodies from Assay Biotechnology (Sunnyvale, CA) and reactive bands were visualized by the addition and excitation of goat anti-rabbit antibodies with Alexa Fluor®546 (Life Technologies) at a 1:5000 dilution (0.2ng/µl) using the Typhoon 9500 Plus laser scanner.

DISCUSSION

A previous study in our laboratory has revealed that A1 and A3 reduce the amount of progeny infectious simian RV (SA11.4f) particles released from the human intestinal cell line (HT29.f8), thus suggesting a decrease in viral replication (Ball et al., 2015). This study investigated changes in a human RV (Wa)-infected African green monkey kidney cell line, MA104, treated with either of the arachidins (A1 or

A3) at 18hpi. Our hypothesis was that the human RV (Wa) replication would be inhibited, and that the ultrastructure of the MA104 cells would be affected by the arachidins.

The viability assay verified that there were no toxic effects on the MA104 cells treated with either of the arachidins (A1 and A3), therefore 20μM concentrations of A1 and A3 and 0.002% DMSO, which was used to solubilize the arachidins, are nontoxic to MA104 cells. It was interesting to observe a significantly increased viability with the addition of DMSO to the untreated cells when compared to RV-infected cells treated with A1 or A3. Although there were no significant differences between RV-infected (no DMSO) and RV-infected cells treated with A1 or A3, there was a significant difference between RV-infected cells treated with A1 and uninfected A3 treated cells, and significant difference between RV-infected cells treated with A1 and NV with DMSO. This infers a possible difference in how A1 modifies an RV infection versus noninfected MA104 cells treated with A1 or DMSO alone.

Likewise, the decreased amount of infectious RV produced in Wa-infected arachidin treated MA104 cells resembled the decrease in progeny RV produced in the simian RV, (SA11.4f)-infected human intestinal cell line (HT29.f8) with arachidin treatments (Ball et al., 2015). This indicated that A1 and A3 have antiviral properties that effect both simian and human RV strains in both African green monkey kidney (MA104) and human intestinal (HT29.f8) cell lines.

TEM examination of intracellular RV particles demonstrated two size populations; the more mature nonenveloped (neRV) that are of similar sizes of mature infectious RV particles and the less mature enveloped (eRV) (Estes and Greenberg, 2013). At the same time point (18hpi), TRPS analysis of extracellular nanoparticles (50-150nm) using the Izon qNano system revealed relatively equal number

of extracellular particles among treatments with and without arachidins, however the size distribution of the particles varied significantly. It is notable that the virus particles observed in the MA104 cells were similar in size to the nanoparticles observed outside the infected cells. This suggests that some of the nanoparticles that are released from RV-infected cells maybe infectious RV particles as these supernatants produced more infectious RV particles (~73nm) than the arachidin treated cells (~110nm) as shown with the plaque forming assays. This suggests that the maturation of the infectious RV particles is affected with the addition of the arachidins (A1 and A3). Previous studies infecting Caco-2 cells with RRV (rhesus monkey rotavirus) have shown the presence of extracellular vesicles (EVs) composed of exosomes and apoptotic bodies obtained by filtration/ultracentrifugation or differential centrifugation (Barreto et al., 2010; Bautista et al., 2015). A recent manuscript has reviewed data that show Picornaviridae and Hepesviridae produce virus particles in fully host-derived lipid bilayers that resemble extracellular vesicles (EV), which are 50 nm–1 μm vesicles released by infected cells (van der Grein et al., 2018). These studies indicate that some of the nanoparticles that our study has measured maybe EVs, therefore they will be further characterized in future studies.

The nucleus to cytoplasm ratios studies and plasma membrane blebbing of the RV-infected MA104 cells showed characteristics of apoptosis similar to that seen in previous studies (Nikoletopoulou et al., 2013), while the appearance of RV-infected cells treated with A1 or A3 was similar to the control cells (NV, A1 and A3 only). This implies cellular alterations to achieve homeostasis.

Additionally, the increased presence of autophagosomes in the MA104 cells with A1 alone and RV with A1 suggested that A1 modulates MA104 cellular homeostasis and RV infections by

stimulating cells to utilize the autophagy pathway. Autophagy is a conserved mechanism that is a safeguard for cellular homeostasis. It produces autophagosomes to degrade damaged proteins in the cytoplasm and is believed to be a pro-survival pathway (Noguchi and Hirata, 2015). However, autophagy can be a form of programmed cell death as demonstrated in a study that shows the activation of cannabinoid receptors induces autophagy mediate cell death through the stimulation of ER stress in human glioma cells (Costa et al., 2016). Autophagy is regulated by several cellular signaling pathways including class I phosphoinositide 3-kinase (PI3K), protein kinase B (PKB)-mammalian target of rapamycin complex 1 (mTORC1), and other mTOR-independent pathways (Chiu et al., 2014). The consequences of the activation of the autophagy depends on the types of cells and the stress-inducing signals (Kenakin and Christopoulos, 2013; Raehal et al., 2005; Rasmussen et al., 2011b, 2011a).

A recent drug screening study has identified the PI3K/mTOR inhibitor, BEZ235, as a regulator of both influenza virus production and cellular metabolic homeostasis (Smallwood, et al, 2017). Proteomic and functional analysis of the primary epithelial cells show a regulation of homeostasis in the infected cells that changes with the addition of BEZ235. Also, BEZ235 protects mice challenged with a lethal dose of influenza. This implies another potential antiviral agent has similar effects on both the virus and the cells. It will be interesting to determine if A1, A3 and BEZ235 use similar mechanism(s) of action.

Previously, a cannabinoid receptor binding study has demonstrated that both A1 and A3 bind to CBR1 and CBR2. Moreover, A3 was shown to be a competitive receptor antagonist for CBR1, and A1 antagonized CBR1 agonists by both competitive and non-competitive mechanisms (Brents et al., 2012). Cannabinoid receptors (CBRs) are G-protein coupled receptors (GPCRs) that are present on many types of cells. They control diverse physiological functions, including neural processes, cellular metabolism, and modulation of cellular activity including apoptosis (Bosier et al., 2010). The GPCRs have been shown to activate different G proteins to inhibit adenylyl cyclase, couple to the mitogen-activated protein kinase (MAPK) pathway, to couple to phospholipase C causing the release of intracellular calcium ($[Ca]_i$), and activate phosphatidylinositide-3-kinase causing the inhibition of voltage-dependent calcium channels (ICa)(Kamato et al., 2017; Khan et al., 2016; Neves et al., 2002). The presence of CBRs on MA104 cells suggests an activation of a receptor-mediated cell signaling pathway(s) that could be used to modulate an RV infection. This implies that the addition of A1 and A3 may initiate biased signaling, which is the activation of different signaling pathways or the same signaling pathways differently (Ibsen et al., 2017). Biased signaling has been defined as the model of how different ligands act on the same GPCR, in the same tissue, can give rise to markedly different cellular responses by stabilizing different receptor conformations. The differential signaling pathway activation by different agonists can also arise as consequences of kinetics. Changes in the timing of dissociation of different ligands may result in receptor conformations that favor low affinity interactions for a particular receptor/signaling molecule pair to produce a signaling cascade (Ibsen et al., 2017).

Also, some of the variability observed in the pathways activating kinases downstream of both CBR1 and CBR2 may be due to the differential expression of the receptors on different cell types. An example of this is presented in a study that shows the requirement of high receptor expression for the activation of pAkt, but the activation of ERK1/2 is not affected by the level of expression of the receptors (Cudaback et al., 2010). Future studies will explain the influence of different cell types, with

different receptor numbers and second messenger expressions used in the cannabinoid receptor signaling pathways. Biased signaling of GPCR-directed therapeutics would allow for a more targeted approach for antiviral treatments.

In summary, this study showed that RV-infected MA104 cells treated with A1 or A3 exhibited a more normal ultrastructural appearance than untreated RV-infected cells; a decrease in the number of extracellular infectious RV particles; a decrease in structural and nonstructural RV proteins; and a shift to a larger size population of extracellular nanoparticles. However, the fact that A1 produced numerous autophagosomes while A3 did not, infers that different mechanism(s) of action or different stimulations of the same mechanism(s) of action modulate an RV infection. This suggests that A1 and A3 have anti-RV activity towards different RV strains and implies potential broad range therapeutic activity on other virus infections that employ similar mechanism(s) of action. Future studies will resolve these differences and disclose the mechanism(s) of action of A1 and A3 that will illustrate their anti-RV therapeutic activity.

REFERENCES

Abbott, J.A., F Medina-Bolivar, E.M Martin, A.S. Engelberth, H. Villagarcia, E.C. Clausen, and D.J Carrier. 2010. Purification of resveratrol, arachidin-1, and arachidin-3 from hairy root cultures of peanut (Arachis hypogaea) and determination of their antioxidant activity and cytotoxicity. Biotechnol. Prog. 26, 1344–1351.

Aggarwal, B.B., A. Bhardwaj, R.S. Aggarwal, N.P. Seeram, S. Shishodia, and Y. Takada. 2004. Role of resveratrol in prevention and therapy of cancer: preclinical and clinical studies. Anticancer Res. 24, 2783–2840.

Akpinar, F. and J. Yin. 2015. Characterization of Vesicular stomatitis virus populations by tunable resistive pulse sensing Fulya. J. Virol. Methods 33, 395–401.

Anderson, E.J. and S.G. Weber. 2004. Rotavirus infection in adults. Lancet Infect. Dis. 4, 91–99.

Arnold, M., J.T. Patton, and S.M. McDonald. 2009. Culturing, Storage, and Quantification of Rotaviruses. Curr. Protoc.Microbiol. 15C.3.1-15C.3.24.

Athar, M., J.H. Back, X. Tang, K.H. Kim, L. Kopelovich, D.R. Bickers, and A.L. Kim. 2007. Resveratrol: a review of preclinical studies for human cancer prevention. Toxicol. Appl. Pharmacol. 224, 274–283.

Bakare, N., D. Menschik, R. Tiernan, W. Hua, and D. Martin. 2010. Severe combined immunodeficiency (SCID) and rotavirus vaccination: Reports to the Vaccine Adverse Events Reporting System (VAERS). Vaccine 28, 6609–6612.

Ball, J.M., F. Medina-Bolivar, K Defrates, E. Hambleton, M.E. Hurlburt, L. Fang, T. Yang, L. Nopo-Olazabal, R.L. Atwill, P. Ghai, and R.D. Parr. 2015. Investigation of Stilbenoids as Potential Therapeutic Agents for Rotavirus Gastroenteritis. Adv. Virol. 2015, 1–10.

Barreto, A., L.-S. Rodríguez, O.L. Rojas, M. Wolf, H.B. Greenberg, M. Franco, and J. Angel. 2010. Membrane vesicles released by intestinal

epithelial cells infected with rotavirus inhibit T-cell function. Viral Immunol. 23, 595–608.

Bautista, D., L.-S. Rodríguez, M.A. Franco, J. Angel, and A. Barreto. 2015. Caco-2 cells infected with rotavirus release extracellular vesicles that express markers of apoptotic bodies and exosomes. Cell Stress Chaperones 20, 697–708.

Bhandari, N., T. Rongsen-Chandola, A. Bavdekar, J. John, K. Antony, S. Taneja, N. Goyal, A. Kawade, G. Kang, S.S. Rathore, S. Juvekar, J. Muliyil, A. Arya, H. Shaikh, V. Abraham, S. Vrati, M. Proschan, R. Kohberger, G. Thiry, R. Glass, H.B. Greenberg, G. Curlin, K. Mohan, G.V.J. Harshavardhan, S. Prasad, T.S. Rao, J. Boslego, and M.K. Bhan. 2014. Efficacy of a monovalent human-bovine (116E) rotavirus vaccine in Indian infants: A randomised, double-blind, placebo-controlled trial. Lancet 383, 2136–2143.

Bo, A.N., E. Pol, and A.E. Van Der, Grootemaat. 2014. Single-step isolation of extracellular vesicles by size-exclusion chromatography. J. Control. Release 1, 1–11.

Bosier, B., G.G. Muccioli, E. Hermans, and D.M. Lambert. 2010. Functionally selective cannabinoid receptor signalling: Therapeutic implications and opportunities. Biochem. Pharmacol. 80, 1–12.

Brents, L.K., F. Medina-Bolivar, K. Seely, V. Nair, S.M. Bratton, L. Ñopo-Olazabal, R.Y. Patel, H. Liu, R.J. Doerksen, P.L. Prather, and A. Radominska-Pandya. 2012. Natural prenylated resveratrol analogs arachidin-1 and -3 demonstrate improved glucuronidation profiles and have affinity for cannabinoid receptors. Xenobiotica 42, 139–156.

Chiu, H.C., S. Richart, F.Y. Lin, W.L. Hsu, and H.J. Liu, 2014. The interplay of reovirus with autophagy. Biomed Res. Int. 2014, 1–8.

Condori, J., G. Sivakumar, J. Hubstenberger, M.C. Dolan, V.S. Sobolev, and F. Medina-Bolivar.

2010. Induced biosynthesis of resveratrol and the prenylated stilbenoids arachidin-1 and arachidin-3 in hairy root cultures of peanut: Effects of culture medium and growth stage. Plant Physiol. Biochem. 48, 310–318.

Costa, L., C. Amaral, N. Teixeira, G. Correia-da-Silva, and B.M. Fonseca. 2016. Cannabinoid-induced autophagy: Protective or death role? Prostaglandins Other Lipid Mediat. 122, 54–63.

Cudaback, E., W. Marrs, T. Moeller, and N. Stella. 2010. The Expression Level of CB1 and CB2 Receptors Determines Their Efficacy at Inducing Apoptosis in Astrocytomas. PLoS One 5, e8702.

DeBlois, R.W. and C.P. Bean. 1970. Counting and sizing of submicron particles by the resistive pulse technique. Rev. Sci. Instrum. 41, 909–916.

Di Fiore, I.J.M., G. Holloway, and B.S. Coulson. 2015. Innate immune responses to rotavirus infection in macrophages depend on MAVS but involve neither the NLRP3 inflammasome nor JNK and p38 signaling pathways.Virus Res. 208, 89–97.

Elmore, S. 2007. Apoptosis: a review of programmed cell death. Toxicol. Pathol. 35, 495–516.

Estes, M.K. and H Greenberg. 2013. Rotaviruses, in: Fields Virology. Wolters Kluwer Health/Lippincott Williams & Wilkins, Philadelphia, PA, pp. 1347–1401.

Farkas, K., L. Pang, S. Lin, W. Williamson, R. Easingwood, R. Fredericks, M. Jaffer, and A. Varsani. 2013. A Gel Filtration-Based Method for the Purification of Infectious Rotavirus Particles for Environmental Research Applications. Food Environ. Virol. 5, 231–235.

Freshney, R.I. 1994. Culture of Animal Cells: A Manual of Basic Technique., 3rd ed. Wiley-Liss, New York.

Halasz, P., G. Holloway, and B.S. Coulson. 2010.

Death mechanisms in epithelial cells following rotavirus infection, exposure to inactivated rotavirus or genome transfection. J. Gen. Virol. 91, 2007–2018.

Harlow, E. and D. Lane. 1988. Antibodies a laboratory manual. Cold Spring Harbor Laboratory Press. pp386-387.

Holloway, G. and B.S. Coulson. 2006. Rotavirus activates JNK and p38 signaling pathways in intestinal cells, leading to AP-1-driven transcriptional responses and enhanced virus replication. J. Virol. 80, 10624–10633.

Holloway, G., T.T. Truong, and B.S. Coulson. 2009. Rotavirus antagonizes cellular antiviral responses by inhibiting the nuclear accumulation of STAT1, STAT2, and NF-kappaB. J. Virol. 83, 4942–4951.

Hsieh, Y.C., F.T. Wu, C.A. Hsiung, H.S. Wu, K.Y. Chang, and Y.C. Huang. 2014. Comparison of virus shedding after lived attenuated and pentavalent reassortant rotavirus vaccine. Vaccine 32, 1199–1204.

Huang, C.-P., L.-C. Au, R.Y.-Y. Chiou, P.-C. Chung, S.-Y. Chen, W.-C. Tang, C.-L., Chang, W.-H. Fang, and S.-B. Lin. 2010. Arachidin-1, a Peanut Stilbenoid, Induces Programmed Cell Death in Human Leukemia HL-60 Cells. J. Agric. Food Chem. 12123–12129.

Ibsen, M.S., M. Connor, and M. Glass. 2017. Cannabinoid CB $_1$ and CB $_2$ Receptor Signaling and Bias. Cannabis Cannabinoid Res. 2, 48–60.

Jiang, V., B. Jiang, J. Tate, U.D. Parashar, and M.M. Patel. 2010. Performance of rotavirus vaccines in developed and developing countries. Hum. Vaccin. 6, 532–542.

Kamato, D., P. Mitra, F. Davis, F., N. Osman, R. Chaplin, P.J. Cabot, R. Afroz, W. Thomas, W. Zheng, H. Kaur, M. Brimble, and P.J. Little. 2017. Gaq proteins: molecular pharmacology and therapeutic potential. Cell.Mol.LifeSci.74, 1379–1390.

Kenakin, T. and A. Christopoulos. 2013. Signalling bias in new drug discovery : detection, quantification and therapeutic impact 12, 205–216.

Khan, S.M., J.Y. Sung, and T.E. Hébert. 2016. Gβγ subunits—Different spaces, different faces. Pharmacol. Res. 111, 434–441.

Kozak, D., W. Anderson, R. Vogel, and M. Trau. 2011. Advances in resistive pulse sensors: Devices bridging the void between molecular and microscopic detection. Nano Today 6, 531–545.

Leshem, E., B. Lopman, R. Glass, J. Gentsch, K. Banyai, U. Parashar, and M. Patel. 2014. Distribution of rotavirus strains and strain-specifi c eff ectiveness of the rotavirus vaccine after its introduction: a systematic review and meta-analysis 14, 847–856.

Matthijnssens, J., M. Ciarlet, E. Heiman, I. Arijs, T. Delbeke, S.M. McDonald, E. Palombo, E., M. Iturriza-Gómara, P. Maes, J.T. Patton, M. Rahman, and M. Van Ranst, M. 2008. Full genome-based classification of rotaviruses reveals a common origin between human Wa-Like and porcine rotavirus strains and human DS-1-like and bovine rotavirus strains. J. Virol. 82, 3204–3219.

Mitchell, D.M. and J.M. Ball. 2004. Characterization of a spontaneously polarizing HT-29 cell line, HT-29/cl.f8. In Vitro Cell. Dev. Biol. Anim. 40, 297–302.

Moss, R., Q. Mao, D. Taylor, and C. Saucier. 2013. Investigation of monomeric and oligomeric wine stilbenoids in red wines by ultra high performance liquid chromatography / electrospray ionization quadrupole time-of-flight mass spectrometry. Rapid Commun. Mass Spectrom.

Neves, S.R., P.T. Ram, and R. Iyengar. 2002. G Protein Pathways. Science (80). 296, 1636–1639.

Nikoletopoulou, V., M. Markaki, K. Palikaras, and N. Tavernarakis. 2013. Crosstalk between apoptosis, necrosis and autophagy. Biochim. Biophys. Acta - Mol. Cell Res. 1833, 3448–3459.

Noguchi, M and N. Hirata. 2015. Intersection of Apoptosis and Autophagy Cell Death Pathways. Austin J. Mol. Cell. Biol. 2, 1–7.

Otto, P.H., J. Reetz, W. Eichhorn, W. Herbst, and M.C. Elschner. 2015. Isolation and propagation of the animal rotaviruses in MA-104 cells—30 years of practical experience. J. Virol. Methods 223, 88–95.

Park, M., Y.J. Yun, S. Woo, J.W. Lee, N.G. Chung, N.G., and B. Cho. 2015. Rotavirus-associated hemophagocytic lymphohistiocytosis (HLH) after hematopoietic stem cell transplantation for familial HLH. Pediatr. Int. 57, e77–e80.

Patel, N.C., P.M. Hertel, M.K. Estes, M. de la Morena, A.M. Petru, L.M. Noroski, P.A. Revell, I.C. Hanson, M.E. Paul, H.M. Rosenblatt, and S.L. Abramson. 2010. Vaccine-acquired rotavirus in infants with severe combined immunodeficiency. N. Engl. J. Med. 362, 314–319.

Patton, J.T. 2012. Rotavirus diversity and evolution in the post-vaccine world. Discov. Med. 13, 85–97.

Raehal, K.M., J.K.L. Walker, and L.M. Bohn. 2005. Morphine Side Effects in β-Arrestin 2 Knockout Mice. J. Pharmacol. Exp. Ther. 314, 1195 LP-1201.

Rasmussen, S.G.F., H.-J. Choi, J.J. Fung, E. Pardon, P. Casarosa, P.S. Chae, P.S., B.T. DeVree, D.M. Rosenbaum, F.S. Thian, T.S. Kobilka, A. Schnapp, I. Konetzki, R.K. Sunahara, S.H. Gellman, A. Pautsch, J. Steyaert, W.I. Weis, and B.K. Kobilka. 2011a. Structure of a nanobody-stabilized active state of the β(2) adrenoceptor. Nature 469, 175–180.

Rasmussen, S.G.F., B.T. DeVree, Y. Zou, A.C. Kruse, K.Y. Chung, T.S. Kobilka, F.S. Thian, P.S. Chae, E. Pardon, D. Calinski, J.M. Mathiesen, S.T.A. Shah, J.A. Lyons, M. Caffrey, S.H. Gellman, J. Steyaert, G. Skiniotis, W.I. Weis, R.K. Sunahara, and B.K. Kobilka. 2011b. Crystal Structure of the β(2)Adrenergic Receptor-Gs protein complex. Nature 477, 549–555.

Roupe, K.A., C.M. Remsberg, J.A. Yanez, and N.M. Davies. 2006. Pharmacometrics of stilbenes: seguing towards the clinic. Curr. Clin. Pharmacol. 1, 81–101.

Saxena, K., S.E. Blutt, K. Ettayebi, X.-L. Zeng, J.R. Broughman, S.E. Crawford, U. Karandikar, N. Sastri, M. Conner, A. Opekun, D. Graham, W. Qureshi, V. Sherman, J. Foulke-Abel, J. In, O., Kovbasnjuk, N. Zachos, M. Donowitz, and M. Estes. 2016. Human Intestinal Enteroids: a New Model To Study Human Rotavirus Infection, Host Restriction, and Pathophysiology. J. Virol. 90, 43–56.

Uzri, D. and H.B. Greenberg. 2013. Characterization of Rotavirus RNAs That Activate Innate Immune Signaling through the RIG-I-Like Receptors. PLoS One 8, 1–15.

van der Grein, S.G., K.A.Y. Defourny, E.F.J. Slot, and E.N.M. Nolte-'t Hoen. 2018. Seminars in Immunopathology Intricate relationships between naked viruses and extracellular vesicles in the crosstalk between pathogen and host. Semin. Immunopathol.

Vogel, R., G. Willmott, D. Kozak, G.S. Roberts, W. Anderson, L. Groenewegen, B. Glossop, A. Barnett, A. Turner,and M. Trau. 2011. Quantitative Sizing of Nano/ Microparticles with a Tunable Elastomeric Pore Sensor. Anal. Chem. 83, 3499–3506.

Ward, R.L. 1996. Mechanisms of protection against rotavirus in humans and mice. J. Infect. Dis. 174 Suppl, S51–S58.

Weatherall, E., P. Hauer, R. Vogel, and G.R.

Willmott. 2016. Pulse Size Distributions in Tunable Resistive Pulse Sensing. Anal. Chem 88, 8648–8656.

Weinberg, G., E.N. Teel, S. Mijatovic-Rustempasic, D.C. Payne, S. Roy, K. Foytich, U.D. Parashar, U.D., J.R. Gentsch, and M.D. Bowen. 2013. Detection of novel rotavirus strain by vaccine post licensure surveillance. Emerg. Infect. Dis. 19, 1321–1323.

Wright, R. 2000. Transmission electron microscopy of yeast. Microsc Res Tech. 51, 496–510.

Yakshe, K.A., Z.D. Franklin, and J.M. Ball. 2015. Rotaviruses: Extraction and Isolation of RNA, Reassortant Strains, and NSP4 Protein, in: Curr. Protoc. Microbiol. 37:15C.6.1-15C.6.44.

Yang, T., L. Fang, and F. Medina-Bolivar. 2017. Biosynthesis and Bioproduction of Bioactive Stilbenoids in Hairy Root Cultures., in: Malik, S. (Ed.), Production of Plant Derived Natural Compounds through Hairy Root Culture. Springer, Cham., pp. 45–64.

Yang, T., L. Fang, C. Nopo-Olazabal, J. Condori, L. Nopo-Olazabal, C. Balmaceda, and F. Medina-Bolivar. 2015. Enhanced Production of Resveratrol, Piceatannol, Arachidin-1, and Arachidin-3 in Hairy Root Cultures of Peanut Co-treated with Methyl Jasmonate and Cyclodextrin. J. Agric. Food Chem. 63, 3942–3950.

Yen, C., K. Bsn, R.N. Jakob, K., M.D. Esona, J. Rausch, J.J. Hull, S. Whittier, and R. Jon. 2015. Detection of Fecal Shedding of Rotavirus Vaccine in Infants Following Their First Dose of Pentavalent Rotavirus Vaccine Catherine. Vaccine 29, 4151–4155.

Yen, C., J.E. Tate, T.B. Hyde, M.M. Cortese, B.A. Lopman, B. Jian, R.I. Glass, R.I., and U.D. Parashar. 2014. RV Vaccines-Current Status and Future Considerations. Hum. Vaccine Immunother. 10, 1–13.

Yin, Y., H.J. Metselaar, D. Sprengers, M.P. Peppelenbosch, and Q. Pan. 2015. Rotavirus in organ transplantation: Drug-virus-host interactions. Am. J. Transplant. 15, 585–593.